

Many-Body-Expansion Based on Variational Quantum Eigensolver and Deflation for Dynamical Correlation

Enhua Xu,¹ Yuma Shimomoto,¹ Seiichiro L. Ten-no,¹ and Takashi Tsuchimochi^{1,2, a)}

¹⁾ Graduate School of System Informatics, Kobe University, 1-1 Rokkodai-cho, Nada-ku, Kobe, Hyogo 657-8501 Japan

²⁾ Japan Science and Technology Agency (JST), Precursory Research for Embryonic Science and Technology (PRESTO), 4-1-8 Honcho Kawaguchi, Saitama 332-0012 Japan

In this study, we utilize the many-body expansion (MBE) framework to decompose electronic structures into fragments by incrementing the virtual orbitals. Our work aims to accurately solve the ground and excited state energies of each fragment using the variational quantum eigensolver and deflation algorithms. Although our approach is primarily based on unitary coupled cluster singles and doubles (UCCSD) and a generalization thereof, we also introduce modifications and approximations to conserve quantum resources in MBE by partially generalizing the UCCSD operator and neglecting the relaxation of the reference states. As a proof of concept, we investigate the potential energy surfaces for the bond-breaking processes of the ground state of two molecules (H_2O and N_2) and calculate the ground and excited state energies of three molecules (LiH , CH^+ , and H_2O). The results demonstrate that our approach can, in principle, provide reliable descriptions in all tests, including strongly correlated systems, when appropriate approximations are chosen. Additionally, we perform model simulations to investigate the impact of shot noise on the total MBE energy and show that precise energy estimation is crucial for lower-order MBE fragments.

I. INTRODUCTION

Finding an approximation to the full configuration interaction (FCI) solution for the many-electron electronic Schrödinger equation remains a challenging task in *ab initio* electronic structure theory, particularly for strongly correlated quantum systems. Several significant advancements have been made in the field of classical computation, such as the density matrix renormalization group method,^{1,2} stochastic approaches in configuration space,³⁻⁵ adaptive coupled cluster (CC) approach,^{6,7} adaptive configuration interaction approaches⁸⁻¹⁰, and the many-body-expansion FCI (MBE-FCI) approach.^{11,12} All of these methods can provide FCI-accuracy results for systems that cannot be processed using FCI. However, because the Hilbert space of quantum systems increases exponentially with the system size, the accuracy of these methods decreases significantly when the tested system becomes larger.

Quantum computation can naturally represent and manipulate quantum states; thus, it is expected to be an effective tool for simulating quantum mechanical systems.¹³⁻¹⁵ Early implementations of quantum algorithms in computational chemistry¹⁶ were deployed on quantum computers to evaluate molecular energies.¹⁷⁻²⁰ Unfortunately, quantum computers are extremely sensitive to errors caused by environmental disturbances, decoherence, and noise. Fault-tolerant quantum computing (FTQC) using quantum error-correcting codes was also investigated.²¹⁻²⁴ However, currently, high-level encoding is not allowed due to restrictions on quantum resources such as qubit and magic state count.^{22,23}

This limitation has been the driving force behind significant progress toward the development of algorithms that seek to reduce the quantum resources for solving quantum chemical problems. Some of these developments include quantum-classical hybrid algorithms for variational optimization^{17,25,26} and wavefunction ansätze that produce low-depth circuits for efficient quantum simulation.²⁷⁻³²

Although quantum computing is expected to be suitable for capturing strong entanglements in a truncated orbital space, an accurate description of the electronic structure also requires the treatment of weak interactions owing to high-lying virtual orbitals. In quantum chemistry, these correlation effects are historically referred to as “static correlation” and “dynamical correlation,” respectively. The latter poses a significant challenge to quantum simulations because the number of qubits available for mapping the active orbital space is usually limited. Therefore, considerable effort has recently been devoted to developing preprocessing approaches that aim to compress a complicated electronic Hamiltonian into a compact active-space representation. Such approaches include double unitary coupled-cluster,^{33,34} transcorrelated,³⁵⁻³⁷ and canonical transcorrelated methods.^{38,39}

Research has also focused on incorporating problem decomposition techniques developed for classical quantum chemistry applications⁴⁰⁻⁴³ into quantum algorithms to further improve the efficiency of simulations of near-term quantum and FTQC devices.⁴⁴⁻⁴⁶ Problem decomposition techniques offer the advantage of decomposing the full electronic structure problem of a molecule into smaller sub-problems that can be solved with fewer qubits and qubit gates, and the aforementioned pre-processed Hamiltonians can be easily combined. Such approaches have a long history, originating from the ap-

^{a)} Electronic mail: tsuchimochi@gmail.com

plication of the Bethe-Goldstone equation⁴⁷ to quantum chemistry in the 1960s.^{48–50} It has been shown that, by decomposing the correlation energy of the molecular system into n -body sub-systems (increments) through the expansion of core^{51–53} or secondary^{11,54,55} orbitals, correlation energies close to the FCI accuracy can be recovered at low values of n in an embarrassingly parallel computation. The latter framework, denoted many-body-expansion FCI (MBE-FCI), was first proposed by Eriksen and Gauss in 2017.¹¹

In this study, we explore a strategy called MBE-VQE that combines the MBE framework and VQE to capture the residual correlation effect missed by the active space approach. A similar approach was used by Verma et al.⁴⁴ where the reference was Hartree-Fock (HF), and the many-body correlation was expanded by VQE using a unitary coupled-cluster with singles and doubles (UCCSD) ansatz.^{56–58} However, we assume the presence of static correlation, for which HF is inadequate, and therefore use VQE within a small active space as the reference. Based on the VQE circuit, we increased the orbital space to estimate the dynamic correlation post-VQE. While it is possible to employ the same ansatz as the reference VQE to correlate with the fragment secondary orbitals, our scheme exploits the educated guess that the most essential description of dynamic correlation requires single and double particle-hole excitations from a reference wave function. Furthermore, we extend the scheme to excited states by adopting Variational Quantum Deflation (VQD),⁵⁹ and demonstrate the feasibility of our approach by computing the vertical excitation energies of three small molecules (LiH, CH⁺ and H₂O) as showcase examples.

The remainder of this paper is organized as follows. Section II introduces the MBE-VQE (MBE-VQD) framework with the employment of the unitary coupled cluster (UCC) ansatz. In Section III, the computational details and results obtained for the tested systems are discussed. Section IV provides a summary of this study and the outlook for future development prospects.

II. THEORY

A. MBE Framework

When describing strongly correlated systems, a linear combination of multiple determinants is typically employed as the reference wavefunction to provide a qualitatively correct description of the entire system. Based on the occupation of an orbital in the reference wavefunction (doubly occupied, partially occupied, or unoccupied), the complete set of spatial molecular orbitals (MOs) can be partitioned into three subsets: core, active, and secondary orbitals. In this study, we employ commonly used indices for the three subsets: I, J, K, L for the core orbitals; w, x, y, z for the active orbitals; and A, B, C, D for the secondary orbitals, as illustrated in

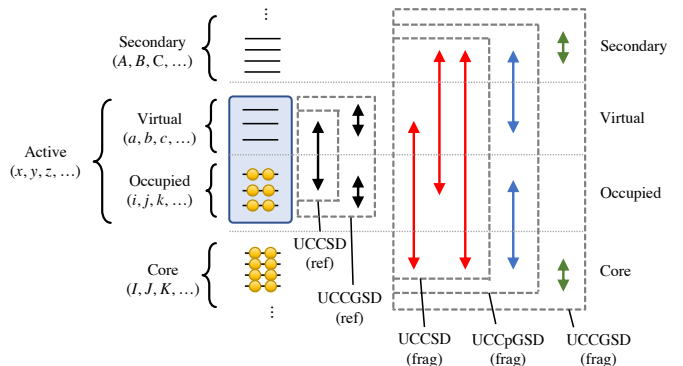


FIG. 1: Schematic illustration of the core, active, and secondary orbitals in the reference wavefunction. The arrows indicate the electron excitations considered in each method that correlate the corresponding spaces.

Figure 1. The active space can be further decomposed into active occupied (i, j, k, l) and active virtual (a, b, c, d) orbitals, given that the initial quantum state is typically an HF state.

In the MBE-FCI method, a complete set of MOs is divided into reference and expansion spaces. In general, the reference space consists of active orbitals, and each fragment includes all active orbitals and a growing number of MOs from the expansion space, which consists of core and secondary orbitals. The residual correlation energy (E_{corr}), defined as the deviation of the reference energy (E_{ref}) from the FCI (E_{FCI}), can be expressed in terms of n body increments as follows:^{12,60–62}

$$\begin{aligned} E_{\text{corr}} &= E_{\text{FCI}} - E_{\text{ref}} \\ &= \sum_p \Delta\epsilon_p + \sum_{p>q} \Delta\epsilon_{pq} + \sum_{p>q>r} \Delta\epsilon_{pqr} + \dots \quad (1) \\ &= E^{(1)} + E^{(2)} + E^{(3)} + \dots \end{aligned}$$

Here, p, q, r are the general indices representing the core or secondary orbitals. $\epsilon_p \equiv \Delta\epsilon_p$ is the correlation energy obtained by performing a calculation on fragment p , which is a composite space of orbital p and active reference space. Similarly, ϵ_{pq} is the correlation energy from fragment p, q . The actual two-body increment of adding orbitals p and q into the reference space simultaneously (denoted as $\Delta\epsilon_{pq}$) is the increment obtained by subtracting ϵ_p and ϵ_q from ϵ_{pq} :

$$\Delta\epsilon_{pq} = \epsilon_{pq} - (\Delta\epsilon_p + \Delta\epsilon_q) \quad (2)$$

Similarly, the three-body increment $\Delta\epsilon_{pqr}$ is computed as follows:

$$\Delta\epsilon_{pqr} = \epsilon_{pqr} - (\Delta\epsilon_p + \Delta\epsilon_q + \Delta\epsilon_r) - (\Delta\epsilon_{pq} + \Delta\epsilon_{pr} + \Delta\epsilon_{qr}) \quad (3)$$

Generally, if the active orbitals are well chosen, most of the static correlation is described in the reference wavefunction, and the remaining dynamic correlation is obtained by calculating the increments of the generated

fragments. Consequently, the MBE expansion in Eqs. (1) converges rapidly. In contrast, an insufficient reference wavefunction may lead to oscillations in the subsequent MBE energies, as discussed in Ref. [55].

From the definition of the increments above, it is clear that the calculation of higher-order approximations to E_{FCI} presupposes knowledge of the components of all contributions at lower orders, in the sense that lower-order increments enter expressions for higher-order increments. Thus, if an error is introduced into the reference energy or a lower-order increment, it is passed on to the corresponding higher-order increments and accumulates in the total energy.

To illustrate the severity of this error accumulation, let us assume that there are M_s secondary orbitals and no core orbitals and that the correlation energies of all the fragments are exactly solved, except for ϵ_A , which is slightly larger than it should be (suppose this error is δ_A). The accuracy of $E^{(1)}$ can be assured as it is lower than its exact value by only δ_A . However, according to Eq. (2), all the two-body increments related to orbital A ($\Delta\epsilon_{AB}$, $\Delta\epsilon_{AC}$, ...) will be δ_A smaller, resulting in $E^{(2)}$ being higher than the exact value by $\delta_A(M_s - 1)$. By analogy, $E^{(3)}$ will be decreased by a much larger magnitude.

This may not be a serious problem in MBE-FCI as all fragment energies may be precisely calculated (assuming that there is no approximation in the FCI solver and round-off errors can be ignored). However, considerable quantum noise in quantum computing, including shot noise, is inevitable at this stage, and even in the foreseeable future. To control its effect on MBE, we consider the following two measures.

The first measure involves freezing the core orbitals and considering only the correlation between the active and secondary orbitals. This is in agreement with earlier MBE-FCI work^{11,54,55}, which was proven to be able to converge at lower orders. Because the error accumulation grows very rapidly as the order increases, such a treatment can effectively control its effect on the total energy.

The second measure entails reducing the shot noise by increasing the number of measurements on the reference and lower-order fragments. In variational quantum computing, the energy expectation value is obtained from the average value of many measurements. Therefore, by performing more measurements, the shot noise can be reduced, but this requires more time. As mentioned above, the noise in the reference or lower-order fragments accumulates more severely than that in the higher-order fragments. Thus, it is cost-effective to perform more measurements on the reference and lower-order fragments, which are also much smaller in number than the high-order fragments. At the end of Section III, we present a model simulation to demonstrate that this treatment is highly efficient.

B. UCC Ansatz

The UCC ansatz takes the exponential form of the anti-hermitized operators \hat{S} ,

$$\hat{S} = \hat{S}_1 + \hat{S}_2 + \dots \quad (4)$$

$$\hat{S}_1 = \sum_{p_1 q_1} t_{q_1}^{p_1} (a_{p_1}^\dagger a_{q_1} - a_{q_1}^\dagger a_{p_1}) \quad (5)$$

$$\hat{S}_2 = \sum_{p_1 p_2 q_1 q_2} t_{q_1 q_2}^{p_1 p_2} (a_{p_1}^\dagger a_{p_2}^\dagger a_{q_2} a_{q_1} - a_{q_1}^\dagger a_{q_2}^\dagger a_{p_2} a_{p_1}) \quad (6)$$

...

where $t_{q_1}^{p_1}$, $t_{q_1 q_2}^{p_1 p_2}$, ... are real parameters and the definition of the orbital spaces for p_1, \dots depends on the method. The most common approach is UCCSD, where \hat{S} contains only single and double substitutions, whose excitations and de-excitations occur only between the occupied and virtual orbitals, like the traditional single-reference CC method (see Fig.1).

Another well-known approach is the UCC with generalized singles and doubles (UCCGSD) ansatz. Unlike UCCSD, the orbital indices in UCCGSD are not limited to occupied or virtual orbitals but are generalized to include all orbitals. Therefore, UCCGSD has more parameters and can provide more accurate results, although it also incurs a higher computational cost. Interestingly, the number of generalized singles and doubles parameters is equal to the number of parameters in the Hamiltonian. As a result, the expectation once existed that the Schrödinger equation could be solved exactly by the coupled cluster method with generalized singles and doubles (CCGSD),⁶³⁻⁶⁶ although this expectation was later proved to be incorrect.⁶⁷⁻⁶⁹ Nevertheless, CCGSD and UCCGSD do deliver much higher performances than CCSD and UCCSD, particularly for describing strongly correlated systems.^{65,66,70}

In our MBE-UCC method, the generation of the reference wavefunction ($|\Psi_{\text{ref}}\rangle$) is formulated as:

$$|\Psi_{\text{ref}}\rangle = e^{\hat{S}_{\text{ref}}} |\Phi\rangle. \quad (7)$$

Here, \hat{S}_{ref} is a specified UCC operator and $|\Phi\rangle$ is set as one determinant in this study. The parameters in \hat{S}_{ref} are optimized to obtain the optimal solution of $|\Psi_{\text{ref}}\rangle$. Then, the fragment wavefunction ($|\Psi_{\text{frag}}\rangle$) is then built upon the optimized $|\Psi_{\text{ref}}\rangle$ as follows:

$$|\Psi_{\text{frag}}\rangle = e^{\hat{S}_{\text{frag}}} |\Psi_{\text{ref}}\rangle = e^{\hat{S}_{\text{frag}}} e^{\hat{S}_{\text{ref}}} |\Phi\rangle \quad (8)$$

where \hat{S}_{frag} is also a UCC operator that can be either the same ansatz as or a different ansatz from \hat{S}_{ref} . Since $|\Psi_{\text{ref}}\rangle$ is considered multi-determinant, this is the unitary version of the so-called ‘‘internally-contracted’’ multi-reference coupled cluster.⁷¹⁻⁷⁴ The quantum circuit for the generation of $|\Psi_{\text{frag}}\rangle$ is illustrated in Figure 2. In our MBE-UCC work, the number of secondary orbitals used in the fragment (denoted as m) is at most three. Thus,

the number of active orbitals (denoted as N) can be easily much larger than m and the corresponding quantum resources, such as qubits and qubit gates related to $e^{\hat{S}_{\text{ref}}}$ will be much greater than those related to $e^{\hat{S}_{\text{frag}}}$.

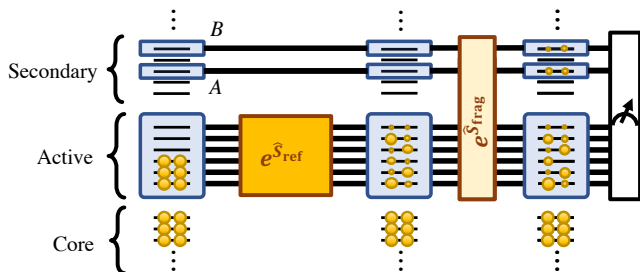


FIG. 2: Schematic quantum circuit diagram of the VQE algorithm for $|\Psi_{\text{frag}}\rangle$ to compute ϵ_{AB} . The initial state is set to a product state representing a single determinant, denoted as $|\Phi\rangle$, whose active space is correlated by the parameterized quantum circuit of $e^{\hat{S}_{\text{ref}}}$. This is then further correlated with orbitals A and B by $e^{\hat{S}_{\text{frag}}}$, followed by the measurements to estimate the energy expectation value.

It should be noted that the parameters \mathbf{t} in $e^{\hat{S}_{\text{ref}}}$ can be fixed or re-optimized in the generation of $|\Psi_{\text{frag}}\rangle$, which are denoted as reference-unrelaxed or reference-relaxed schemes, respectively. The former can be considered an approximation to the latter one.

If \hat{S}_{ref} and \hat{S}_{frag} are both UCCSD (UCCGSD) operators, the resulting approach is denoted MBE-UCCSD (MBE-UCCGSD). Upon convergence, these methods are expected to provide the energy of the corresponding method for a large basis set.

Although the framework of the original MBE is well established and is expected to be transferable to VQE, we aim to reduce the cost of both quantum resources and classical optimization in VQE by introducing the following approximations to make the approach even more feasible: the use of a single trotter step, partial generalization of the UCCSD operator, and fixing the reference $|\Psi_{\text{ref}}\rangle$ in the fragment computation.

1. Single Trotter Step

The first approximation concerns the implementation of the exponential ansatz, $e^{\hat{S}_{\text{frag}}}$ and $e^{\hat{S}_{\text{ref}}}$ as a quantum circuit. In order to make the UCC operator programmable on a quantum device, Trotterization is required for noncommutative exponents.^{56,75,76} Applying UCCSD or UCCGSD to strongly correlated systems often triggers large t amplitudes to account for higher excitations, which, in turn, necessitates a large Trotter number μ , thereby requiring a high-depth quantum circuit. Fortunately, many authors have found that the Trotter

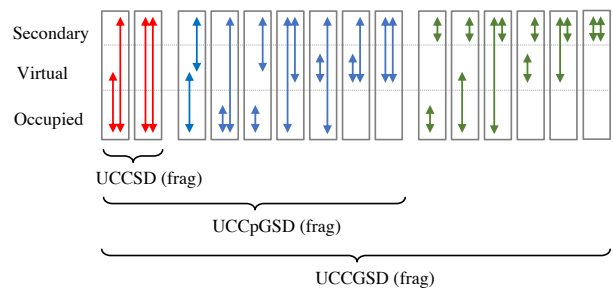


FIG. 3: Types of double substitutions that are considered in \hat{S}_{frag} for each method. The core space is not presented for simplicity.

approximation with $\mu = 1$ can be used, because the variational optimization of the VQE energy can absorb the Trotter error even at $\mu = 1$.^{75,77,78} This is the so-called single Trotter step,⁷⁵ and all the calculations in this work are implemented with this Trotter approximation.

2. Partially Generalized UCCSD Operator

The second approximation concerns the simplification of $e^{\hat{S}_{\text{frag}}}$ in the MBE-UCCGSD. As mentioned previously, fragment computation is expected to capture the dynamical correlation missing from $|\Psi_{\text{ref}}\rangle$. Therefore, we consider it possible to use a modified UCCGSD operator instead of the costly UCCGSD operator for \hat{S}_{frag} in MBE-UCCGSD, in which the occupied orbital indices run over the core and active orbitals, whereas the virtual orbital indices run over the active and secondary orbitals, except for excitations in the active space, as shown in Figure 1. For clarity, we summarize the double substitutions considered for each method in Figure 3 (the core space is excluded for simplicity). This modification can be considered as a kind of "partially generalized" UCCSD (UCCpGSD),⁷⁹ an approach usually exercised in internally-contracted multi-reference methods, and the resulting MBE approach is denoted as MBE-UCCGSD/UCCpGSD.

We also considered employing the UCCpGSD operator \hat{S}_{frag} in MBE-UCCSD. However, this MBE-UCCSD/UCCpGSD results in severe inconsistency in the treatment of the correlation effect between $|\Psi_{\text{ref}}\rangle$ and $|\Psi_{\text{frag}}\rangle$ because the latter can refine the description of the active space in the presence of active-to-active-type excitations (blue arrows in Figure 3). Specifically, compared with MBE-FCI, MBE-UCCSD/UCCpGSD provides fragment total energies that are relatively more accurate than the reference UCCSD energy E_{ref} . This leads to less accurate and overestimated fragment correlation energies ϵ_p , ϵ_{pq} , etc.

In contrast, the inconsistency resulting from the partial generalization in MBE-UCCGSD/UCCpGSD is expected to be much smaller because the correlation ef-

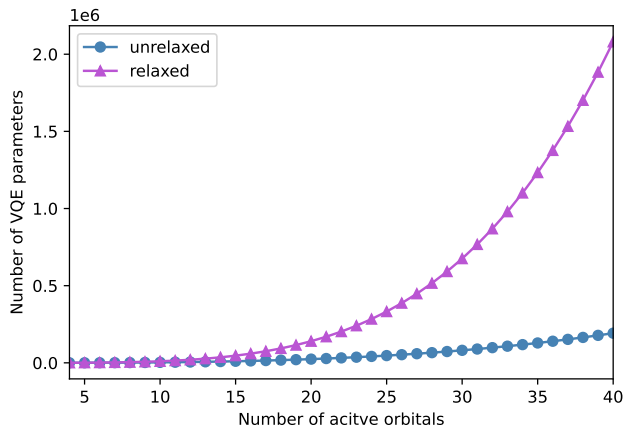


FIG. 4: Number of VQE parameters under the reference-relaxed and reference-unrelaxed approaches in the fragment that includes only one secondary orbital with respect to a different number of active orbitals.

fect missing from the method is typically negligible; core-to-core and secondary-to-secondary excitations in MBE-UCCGSD (green arrows in Figure 3) make negligible contributions to the correlation energy if the active space is well chosen. We return to this point in Section III B.

3. Reference-unrelaxed approximation

The third is the reference-unrelaxed approximation mentioned above, which can lower the cost of optimizing $e^{\hat{S}_{\text{ref}}}$ when computing the fragment. When the number of active orbitals N is much greater than the number of additional fragment orbitals m , $N \gg m$, the reference-unrelaxed scheme can significantly reduce the number of UCC parameters that would need to be optimized in MBE-UCCGSD/UCCpGSD from $O(N^2(N+m)^2)$ to $O(2mN^3)$. Figure 4 shows the number of VQE parameters under the reference-relaxed and reference-unrelaxed approaches with respect to different numbers of active orbitals N for fragment calculation with one secondary orbital ($m = 1$). As is evident from the figure, the larger the active space, the higher the proportion of VQE parameters that can be saved. For example, in a situation with more than 37 active orbitals, the reference-unrelaxed approximation can save more than 90% of the parameters. Such substantial savings in the optimization cost would be highly beneficial to the stability of quantum computing. It should be mentioned that the number of parameters in the reference-unrelaxed MBE-UCCGSD scales as $O(4mN^3)$, which indicates that under this approximation, the UCCpGSD operator would lower the optimization cost to approximately half of its original value.

We realized that the reference-unrelaxed approximation can occasionally introduce some error in the frag-

ment correlation energy and also found that this error can be significantly suppressed by employing optimized orbitals. This is discussed in detail in Section III.

C. Excited states

In the framework of variational quantum algorithms, considerable efforts have been made to obtain excited states.^{80–90} Among them, the most prominent approach is perhaps variational quantum deflation (VQD),⁸² which introduces the following modification to the Hamiltonian to determine the κ th excited state:

$$\hat{H}^{(\kappa)} = \hat{H} + \sum_{\lambda=0}^{\kappa-1} \alpha |\Psi_{\lambda}\rangle \langle \Psi_{\lambda}| \quad (9)$$

This modified Hamiltonian ensures approximate orthogonality between $|\Psi_{\lambda}\rangle$ ($\lambda = 0, 1, 2, \dots, \kappa$), which are the ground state, and the first, second, \dots , and κ th excited states, obtained by the corresponding VQE calculations.

MBE-VQE can be easily generalized to MBE-VQD for excited-state calculations by replacing the Hamiltonian with $\hat{H}^{(\kappa)}$. However, one caveat is that the HF orbitals typically employed for quantum simulations, such as VQE (and VQD), are optimized with respect to the ground state but not for excited states. This leads to an imbalance between the ground and excited states, resulting in a qualitatively incorrect description of the excitation energies at low MBE orders.

To address this issue, we introduced orbital optimization in the reference VQE and VQD states. The orbital-optimized (oo) VQE is similar to the complete active space self-consistent field (CASSCF) and can be classically performed using first- and second-order reduced density matrices.^{91,92} To generalize the orbital optimization to VQD, we simply take the state-average approach where the sum of the VQE and VQD energies is minimized by appropriate orbital rotation. As shown below, with optimized orbitals, the ground- and excited-state energies converge faster than those with HF orbitals with respect to the order of MBE.

III. RESULTS

A. Computational Details

Both MBE-FCI and MBE-UCC were implemented in our Python-based emulator package QUKET,⁹³ which complies with other useful libraries such as OPENFERMION,⁹⁴ PYSCF,⁹⁵ and QULACS.⁹⁶ The Jordan-Wigner transformation⁹⁷ was employed to map the fermion operators to the qubit representation, and the tapering-off technique for reducing the number of qubits was used.^{98,99} We did not consider quantum noise in our calculations. In some calculations, the orbitals (including the core orbitals) were optimized. For cases where FCI

TABLE I: Ground state energies of CH^+ with the aug-cc-pVDZ basis set provided by different approaches. The MBE-FCI energies are in a.u., whereas the deviations of other approaches from MBE-FCI are in mH (milliHartree).

	FCI	UCCSD	UCCSD/UCCpGSD	UCCGSD	UCCGSD/UCCpGSD
Ref	-37.925641	0.008	0.008	0.000	0.000
MBE(1)	-37.973872	0.360	-0.190	0.000	0.000
MBE(2)	-38.005191	1.053	2.276	0.000	-0.001
MBE(3)	-38.005066	1.667	-17.429	0.000	0.004

is unavailable, the multi-reference configuration interaction with Davidson correction (MRCI+Q) energies^{100–102} based on either the HF or CASSCF orbitals were used as the benchmark. In the following applications, we employ MBE-VQE to describe the potential energy surfaces (PESs) for the bond dissociation processes of the ground state of two molecules (H_2O and N_2), and employ both MBE-VQE and MBE-VQD to calculate the ground- and excited-state energies of three molecules (LiH , CH^+ and H_2O). All the data shown below were computed using the reference-unrelaxed approximation, unless otherwise noted. The results of the reference-relaxed scheme are listed in the Supplementary Information (SI).

B. Comparison of MBE methods

We first investigate the performance of MBE using different ansätze using the ground state of the CH^+ molecule as an example. The bond length is 1.131 Å and we use the HF orbitals with the aug-cc-pVDZ basis set. The $1s$ core orbital is frozen and the next five orbitals are selected as the active orbitals. Table I presents the ground state energies calculated by MBE(n)-FCI and the energy differences of the four proposed "reference-relaxed" MBE(n)-UCC approaches, where n indicates the order of expansion.

As shown in the table, MBE(3)-FCI almost converges, given that the FCI energy is -38.004247 Hartree. The MBE(1)-UCCSD/UCCpGSD energy is slightly lower than that of MBE(1)-FCI because of the slightly larger fragment correlation energy $\{\Delta\epsilon_A\}$. As indicated in Section II B 2, the second- and third-order MBE-UCCSD/UCCpGSD energies increasingly deviate from the MBE-FCI results in opposite directions, implying the divergence of the higher-order MBE energies. In contrast, the energies of MBE-UCCSD did not oscillate because of the consistent treatment of the correlation effects, with a reasonably accurate energy of -38.003399 Hartree at third order.

Both MBE-UCCGSD and MBE-UCCGSD/UCCpGSD performed quite well for this system; the accuracy of the former is essentially equivalent to that of MBE-FCI, and the largest deviation of the latter from MBE-FCI is a mere 0.004 mH at the third order. Notably, the energy oscillation in MBE-UCCGSD/UCCpGSD is drastically suppressed

compared to that of MBE-UCCSD/UCCpGSD, and its performance is almost the same as that of MBE-UCCGSD. This clearly demonstrates that the missing correlation effect in UCCpGSD, that is, secondary-to-secondary excitations, has almost no contribution and can be practically neglected. Therefore, in the remainder of this paper, we report and compare only the results of MBE-UCCSD and MBE-UCCGSD/UCCpGSD.

C. Potential Energy Surface

1. H_2O

Next, we examine the bond-breaking process of H_2O using the aug-cc-pVDZ basis set. The H-O-H angle was fixed at 104.33° and the two O-H bonds were varied from 0.9 Å to 3.0 Å. We froze the $1a_1$, $2a_1$, and $1b_1$ orbitals and chose the $3a_1$, $1b_2$, $4a_1$, and $2b_2$ orbitals as the active space. The absolute energies and their deviations from MRCI+Q of the different methods are depicted in Figure 5. As illustrated in Figures 5a and 5b, MBE-UCCSD and MBE-UCCGSD/UCCpGSD exhibit similar behavior at the reference and first order. However, for the second and third orders, MBE-UCCGSD/UCCpGSD is notably closer to MRCI+Q than MBE-UCCSD is, particularly in the bond-breaking region. This highlights the superior ability of MBE-UCCGSD/UCCpGSD compared with MBE-UCCSD in describing strongly correlated systems. The accuracy and convergence of MBE-UCCGSD/UCCpGSD can be further improved by optimizing the orbitals during the reference UCCGSD calculation, which is denoted as ooUCCGSD. Accordingly, the benchmark MRCI+Q is based on CASSCF orbitals. The improvement in MBE-ooUCCGSD/UCCpGSD over MBE-UCCGSD/UCCpGSD was significant, as shown in Figure 4c. We present the maximum absolute error (MAE) and non-parallelity error (denoted as NPE, which refers to the difference between the maximum and minimum deviations) with respect to MRCI+Q for the MBE(2) and MBE(3) data in Table II. Surprisingly, even MBE(2)-ooUCCGSD/UCCpGSD exhibits much smaller MAE and NPE values than MBE(3)-UCCSD and MBE(3)-UCCGSD/UCCpGSD. The overwhelming advantage of MBE-ooUCCGSD/UCCpGSD illustrates the effectiveness of orbital optimization.

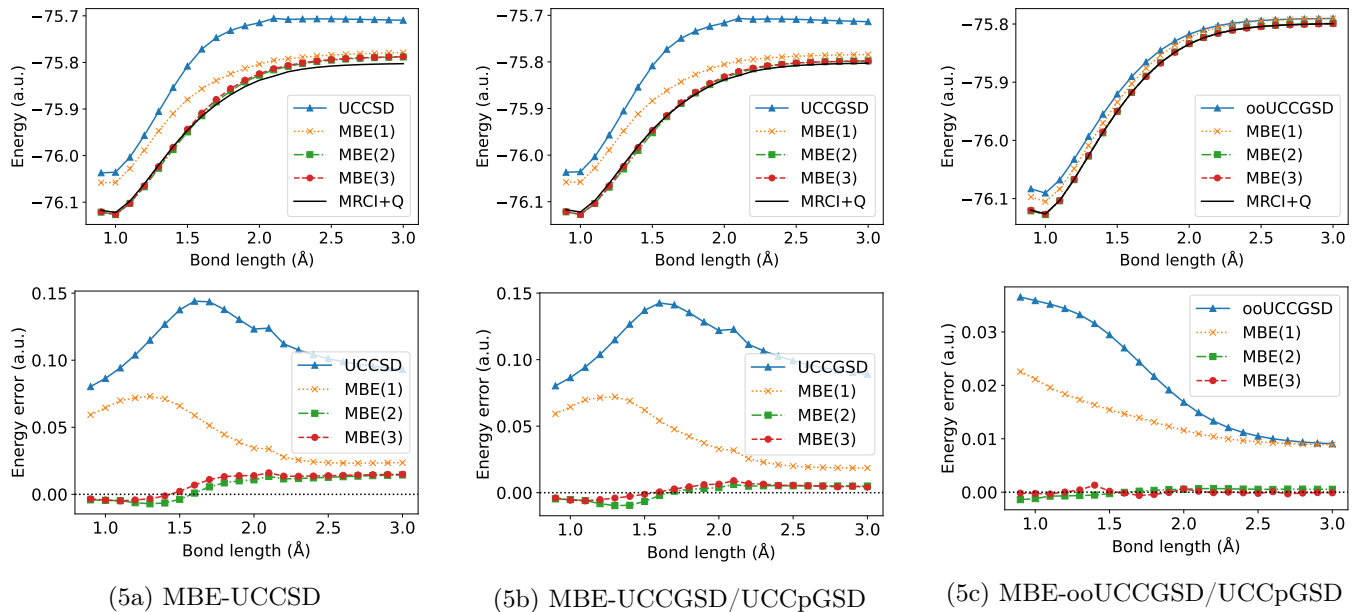


FIG. 5: Absolute and relative (with respect to MRCI+Q) energies of different approaches in the bond dissociation process of the ground state of H_2O with the aug-cc-pVDZ basis set.

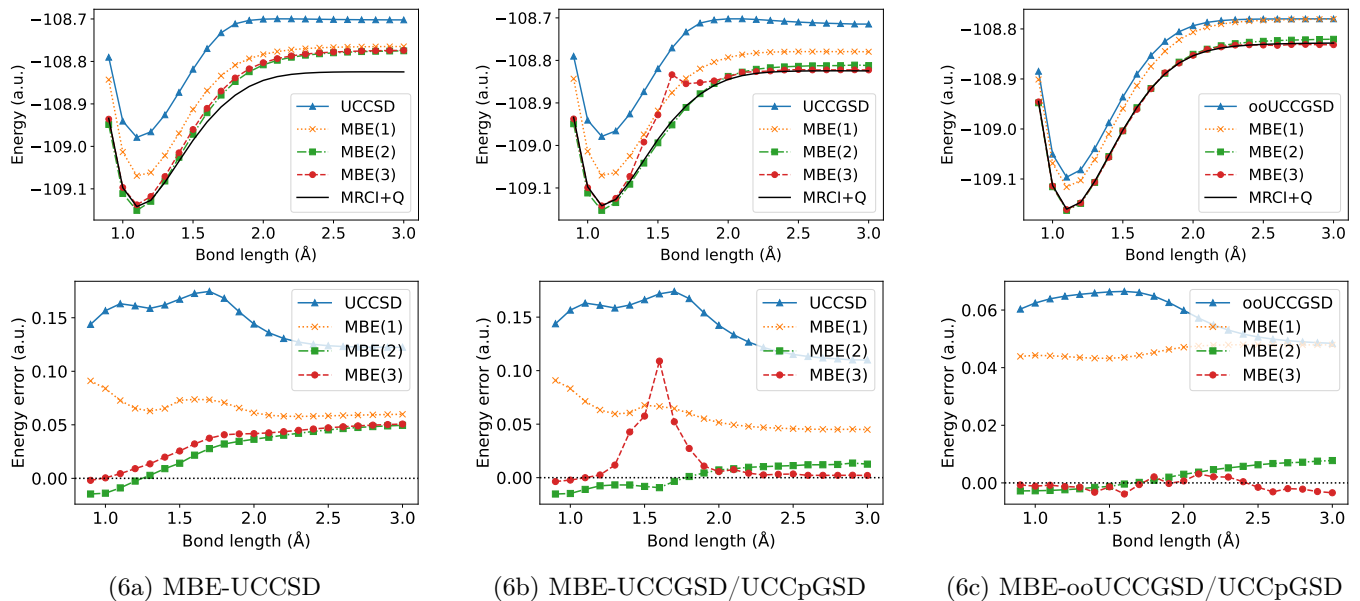


FIG. 6: Absolute and relative (with respect to MRCI+Q) energies of different approaches in the bond dissociation of the ground state of N_2 with the aug-cc-pVDZ basis set.

2. N_2

The PES of the triple bond breaking process of the ground state of N_2 is more challenging to describe accurately than that of H_2O . The aug-cc-pVDZ basis set was employed and the N-N bond was stretched from 0.9 Å to 3.0 Å. The $1\sigma_g, 2\sigma_g, 1\sigma_u$ and $2\sigma_u$ orbitals were frozen and the $1\pi_u, 2\pi_u, 3\sigma_g, 1\pi_g, 2\pi_g,$ and $3\sigma_u$ orbitals were chosen to be active. According to Figures 6a and 6b, the performances of MBE-UCCSD and MBE-

UCCGSD/UCCpGSD are similar to those in Figures 5a and 5b, except that the MBE(3)-UCCGSD/UCCpGSD energies around 1.6 Å are quite different from the benchmark MRCI+Q energies. As listed in Table III, the MAE and NPE values of MBE(3)-UCCGSD/UCCpGSD are as high as 108.9 and 112.5 mH, respectively. However, as shown in Figure S2b and Table SII in SI, the PES of the reference-relaxed MBE(3)-UCCGSD/UCCpGSD is very close to the benchmark results, where the MAE and NPE values are only 3.3 and 6.5 mH, respectively. As they are

both performed on the same HF orbitals, such abnormally different performances can only be attributed to the reference-unrelaxed approximation.

On the other hand, using the optimized orbitals, the PES of MBE(3)-ooUCCGSD/UCCpGSD in Figure 6c becomes very close to the benchmark, and its MAE and NPE values are only 3.9 and 7.0 mH, respectively. This performance demonstrates that the error caused by the reference-unrelaxed approximation is mainly attributed to the inadequate description of the HF orbitals, especially when the system is strongly correlated, and can be significantly suppressed by employing the optimized orbitals.

To enable a clear visualization of the errors from the reference-unrelaxed approximation, we plot the energy deviations of each fragment between the reference-unrelaxed and reference-relaxed approaches in MBE-UCCGSD/UCCpGSD in Figure 7 (with HF orbitals) and 8 (with optimized orbitals). The upper and lower plots represent N_2 at $R = 1.0 \text{ \AA}$ and $R = 1.6 \text{ \AA}$, respectively. First, the energy deviations in the upper figures are always smooth, indicating that the errors from the reference-unrelaxed approach at $R = 1.0 \text{ \AA}$ are insignificant. In contrast, at $R = 1.6 \text{ \AA}$ with HF orbitals, as shown in Figure 7, the deviation for the fragment containing the $5\sigma_u$ secondary orbital, ca. 0.5 mH, is significantly larger than the others. Because of this fragment, all the higher-order fragments that include the $5\sigma_u$ orbital have significantly larger deviations, as shown in Figures 7e and 7f. The resulting MBE(2)-UCCGSD/UCCpGSD and MBE(3)-UCCGSD/UCCpGSD energies are 9.6 mH lower and 108.6 mH higher than the corresponding reference-relaxed energies, respectively. In contrast, after employing the optimized orbitals, the energy deviations in Figure 8 become much smaller. The physical reason for this is that the HF orbitals are not well suited for describing multi-reference systems, and the $5\sigma_u$ secondary orbital in the HF solution correlates significantly with the active space, that is, the active space is not well chosen in this particular case. After orbital optimization, the newly defined active space was well-separated from the secondary space; thus, errors from the reference-unrelaxed approximation were significantly suppressed.

TABLE II: MAE and NPE with respect to MRCI+Q in the PES for the bond dissociation process of the ground state of H_2O . The aug-cc-pVDZ basis set is employed and all the data are in mH (milliHartree).

	MAE	NPE
MBE(2)-UCCSD	14.5	21.5
MBE(3)-UCCSD	16.0	20.9
MBE(2)-UCCGSD/UCCpGSD	9.7	15.9
MBE(3)-UCCGSD/UCCpGSD	9.0	15.1
MBE(2)-ooUCCGSD/UCCpGSD	1.4	2.1
MBE(3)-ooUCCGSD/UCCpGSD	1.3	1.9

TABLE III: MAE and NPE with respect to MRCI+Q in the PES of the bond dissociation of the ground state of N_2 . The aug-cc-pVDZ basis set is employed and all the data are in mH

	MAE	NPE
MBE(2)-UCCSD	49.5	64.2
MBE(3)-UCCSD	50.7	52.6
MBE(2)-UCCGSD/UCCpGSD	15.3	28.9
MBE(3)-UCCGSD/UCCpGSD	108.9	112.5
MBE(2)-ooUCCGSD/UCCpGSD	7.8	10.5
MBE(3)-ooUCCGSD/UCCpGSD	3.9	7.0

TABLE IV: Reference-relaxed and reference-unrelaxed MBE-UCCGSD/UCCpGSD energies at each order with the optimized orbitals for N_2 at 1.6 \AA are listed. The absolute energies are in a.u., and the energy deviations are in mH.

	relax	unrelax	ΔE
MBE(1)	-108.913559	-108.913420	0.139
MBE(2)	-108.957293	-108.957362	-0.069
MBE(3)	-108.958453	-108.960825	-2.372

It should be noted that the error from the reference-unrelaxed approximation cannot be completely eliminated, even by employing optimized orbitals, and these errors will continue to accumulate as the MBE order increases. As listed in Table IV, the deviation between the reference-unrelaxed and reference-relaxed MBE-UCCGSD/UCCpGSD approaches with optimized orbitals significantly increases at the third order. However, we still prefer to retain this approximation, as it can significantly lower the cost of optimizing the fragment computation. The error caused by the reference-unrelaxed approximation is expected to be significantly suppressed by reasonably enlarging the active space.

D. Vertical Excitation Energy

After testing the ground-state energies during the bond-breaking process, we now investigate the vertical excitation energies by employing both the MBE-VQE and MBE-VQD algorithms. All calculations presented in this section were performed using the state-averaged optimized orbitals.

1. LiH

The first molecule is the four-electron system LiH. We considered a stretched bond length of 4.8 \AA with the cc-pVDZ basis set, for which the FCI results have been reported in Ref. 103. The active space containing the

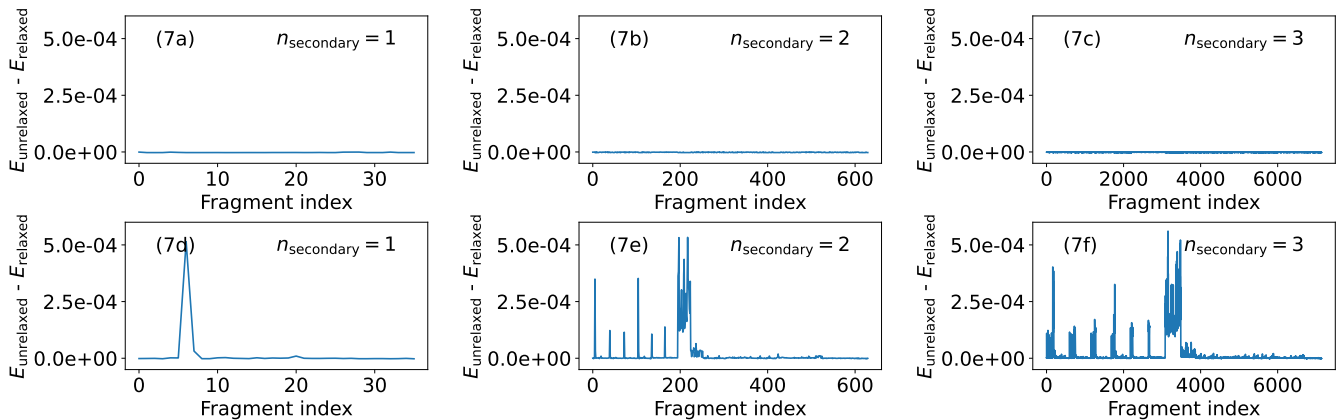


FIG. 7: Energy deviations of each fragment in MBE-UCCGSD/UCCpGSD between reference-unrelaxed and reference-relaxed of N_2 at 1.0 Å and 1.6 Å based on HF orbitals.

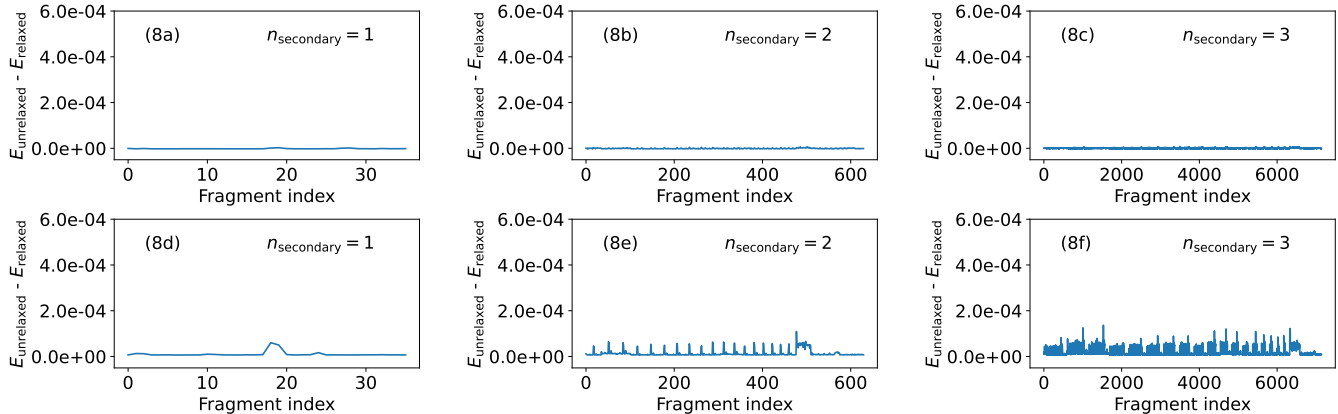


FIG. 8: Energy deviations of each fragment in MBE-UCCGSD/UCCpGSD between the reference-unrelaxed and reference-relaxed approaches of N_2 at 1.0 Å and 1.6 Å with optimized orbitals.

four lowest σ -orbitals was optimized in the reference calculations. Although there are several dominant determinants in the reference wavefunction ($|\Psi_{\text{ref}}\rangle$) of the three lowest Σ^+ states ($1^1\Sigma^+$, $1^3\Sigma^+$, $2^1\Sigma^+$), this is still a simple system with only two active electrons in a chemical sense. Both UCCSD and UCCGSD can provide highly accurate descriptions of $|\Psi_{\text{ref}}\rangle$ and the following MBE-UCCSD and MBE-UCCGSD/UCCpGSD results are satisfactory. As listed in Table V, they provide the exact vertical excitation energy, even for the first order. The absolute energies of MBE-UCCGSD/UCCpGSD are almost the same as those of MBE-FCI, and the maximum deviation between MBE-UCCSD and MBE-FCI is 0.007 meV.

When the HF orbitals are employed without optimization, MBE-UCCGSD/UCCpGSD can still provide accurate excitation energies. However, we found that the description of MBE-UCCSD for $1^3\Sigma^+$ is problematic; the excitation energies of MBE(1), MBE(2), and MBE(3) orders are 0.08, -0.23 and 0.50 eV, respectively. This poor

performance is attributed to the fact that the HF orbitals were optimized for the singlet ground state; hence, the UCCSD operator cannot reasonably describe the triplet excited state.

2. CH^+

The second molecule is CH^+ and we use the same computational conditions as in Section III B. The FCI energies for the three investigated states ($1^1\Sigma^+$, $1^1\Delta$, and $2^1\Sigma^+$) were obtained using the MOLPRO software.¹⁰⁴ The ground state ($1^1\Sigma^+$) is a typical single-reference system, whereas the excited states ($1^1\Delta$ and $2^1\Sigma^+$) have two equally dominant doubly-excited determinants but with different signs. The results are tabulated in Table VI. As we have seen, MBE-UCCSD is unable to describe a strong correlation; it can provide reasonable descriptions of the ground state, but performs very poorly for

TABLE V: MBE energies calculated by different approaches for the ground state ($1^1\Sigma^+$) and two excited states ($1^3\Sigma^+$, $2^1\Sigma^+$) of LiH with the cc-pVDZ basis set. The ground state energies are in a.u. and the vertical excitation energies are in eV.

State	$1^1\Sigma^+$	$1^3\Sigma^+$	$2^1\Sigma^+$
MBE-UCCSD			
Ref	-7.932325	0.02	1.67
MBE(1)	-7.932493	0.03	1.64
MBE(2)	-7.932521	0.03	1.64
MBE(3)	-7.932521	0.03	1.64
MBE-UCCGSD/UCCpGSD			
Ref	-7.932329	0.02	1.67
MBE(1)	-7.932577	0.03	1.64
MBE(2)	-7.932675	0.03	1.64
MBE(3)	-7.932667	0.03	1.64
MBE-FCI			
Ref	-7.932329	0.02	1.67
MBE(1)	-7.932578	0.03	1.64
MBE(2)	-7.932671	0.03	1.64
MBE(3)	-7.932672	0.03	1.64
FCI	-7.933503	0.03	1.64

the excited states, particularly in $1^1\Delta$ of which the reference wavefunction does not have an HF component. In contrast, the MBE-UCCGSD/UCCpGSD absolute energies are much more accurate, and the largest deviation from MBE-FCI is only 0.014 meV. The vertical excitation energies estimated with MBE-UCCGSD/UCCpGSD are almost the same as those estimated with MBE-FCI. This significantly different performance shows that MBE-UCCGSD/UCCpGSD is much more reliable than MBE-UCCSD in describing strongly correlated systems. Even with HF orbitals, the MBE-UCCGSD/UCCpGSD energies are very close to MBE-FCI. Nevertheless, both converge to FCI rather slowly. The energy deviations of MBE-UCCGSD/UCCpGSD at each order relative to FCI with the optimized and HF orbitals are listed in Table VII. When the optimized orbitals are used, the largest deviations at the second- and third-order are only 2.05 and 0.68 mH, respectively. In contrast, for the HF orbitals, the smallest deviation at the third order is 5.38 mH. This faster convergence rate of MBE as a result of orbital optimization can lower both the computational cost and the error accumulation of MBE effectively.

3. H₂O

The last system we considered is a water molecule with the aug-cc-pVDZ basis set. The geometry and extrapolated FCI (exFCI) data were obtained from Ref. 105. The $O1s$ orbital was frozen and the next six

TABLE VI: MBE energies calculated by different approaches for the ground state ($1^1\Sigma^+$) and two excited states ($1^1\Delta$, $2^1\Sigma^+$) of CH⁺ with the aug-cc-pVDZ basis set. The ground state energies are in a.u. and the vertical excitation energies are in eV.

State	$1^1\Sigma^+$	$1^1\Delta$	$2^1\Sigma^+$
MBE-UCCSD			
Ref	-37.954326	7.28	9.00
MBE(1)	-37.992159	7.96	9.07
MBE(2)	-38.002705	6.73	9.91
MBE(3)	-38.002101	17.93	8.20
MBE-UCCGSD/UCCpGSD			
Ref	-37.954315	7.27	8.66
MBE(1)	-37.992902	6.86	8.58
MBE(2)	-38.004999	6.83	8.43
MBE(3)	-38.003943	6.85	8.39
MBE-FCI			
Ref	-37.954315	7.27	8.66
MBE(1)	-37.992905	6.86	8.58
MBE(2)	-38.004948	6.83	8.42
MBE(3)	-38.004445	6.86	8.40
FCI	-38.004247	6.87	8.42

TABLE VII: Energy deviations of MBE-UCCGSD/UCCpGSD relative to FCI with the optimized and HF orbitals. The data are in mH.

State	$1^1\Sigma^+$		$1^1\Delta$		$2^1\Sigma^+$	
	optimized	HF	optimized	HF	optimized	HF
Ref	49.93	74.07	64.83	109.17	58.88	97.13
MBE(1)	11.35	16.20	11.01	11.38	17.38	34.90
MBE(2)	-0.75	4.57	-2.05	3.24	-0.52	12.89
MBE(3)	0.30	5.38	-0.47	8.58	-0.68	8.41

lowest orbitals were used as the active space with orbital optimization. Similar to the CH⁺ case, its ground state (1^1A_1) is a typical single-reference system, and the two excited states (1^3A_1 and 2^1A_1) have two equally dominant determinants, but with different signs. Here, only the MBE-UCCGSD/UCCpGSD approach was employed. In Table VIII, the excitation energy of MBE(3)-UCCGSD/UCCpGSD deviates only by 0.16 eV from that of MBE(3)-FCI, with the largest deviation between their absolute energies being 0.089 meV. Considering that they converged to different targets (UCCGSD and FCI), it is reasonable to assume that more significant deviations occur in larger systems. Because the excitation energy of MBE(3)-UCCGSD/UCCpGSD is only slightly lower than that of FCI and the computational cost increases significantly in the fourth order, truncation of the MBE-UCCGSD/UCCpGSD approach at the third order should be a good compromise for describing the vertical excita-

TABLE VIII: Energies of various approaches at different MBE orders for the ground state (1^1A_1) and two excited states (1^3A_1 and 2^1A_1) of water with the aug-cc-pVDZ basis set. The ground state energies are in a.u. The vertical excitation energies are in eV.

State	1^1A_1	1^3A_1	2^1A_1
MBE-UCCGSD/UCCpGSD			
Ref	-76.040609	8.47	9.03
MBE(1)	-76.161789	9.64	9.98
MBE(2)	-76.288790	9.84	10.27
MBE(3)	-76.270582	9.34	9.66
MBE-FCI			
Ref	-76.040609	8.47	9.03
MBE(1)	-76.161803	9.64	9.98
MBE(2)	-76.288923	9.83	10.25
MBE(3)	-76.273263	9.35	9.82
exFCI		9.49	9.94

tion energies in large systems.

IV. EFFECT OF SHOT NOISE

As we mentioned in Section II, quantum noise, including shot noise, is inevitably present and is included in the total energy. Here, the simulation presented here was therefore designed to quantify the impact of statistical errors caused by shot noise based on the MBE-FCI data for the ground state of water with HF orbitals. Suppose that the noisy energy in fragment X is:

$$e_{X(\text{noise})} = e_X + \epsilon_X \quad (10)$$

where X is the composite index that stands for the fragment, e_X is the exact fragment energy, and ϵ_X represents the corresponding shot noise. In the simulation, ϵ_X is set as a random number between $[-\epsilon, +\epsilon]$, where ϵ is the controlled maximum statistical error and is a constant. Eq. (10) can be used to calculate all noise increments. The resulting noise MBE(2)-FCI and MBE(3)-FCI energies are denoted as $E_2(\text{noise})$ and $E_3(\text{noise})$, respectively. The exact MBE(2)-FCI (-76.29904) and MBE(3)-FCI (-76.27949) energies were used as accurate references. The simulation was run 300 times with different values of ϵ . The probability plots of the deviations of $E_2(\text{noise})$ and $E_3(\text{noise})$ from the corresponding reference with respect to different ϵ values are shown in Figure 9. In the left three plots in Figure 9, ϵ is fixed at each MBE order, the values of which are set to 2×10^{-5} , 1×10^{-5} and 5×10^{-6} Hartree, respectively. In the rightmost plot, we use a varying ϵ , denoted as ϵ^* , which is set to 1×10^{-6} , 2×10^{-6} , 1×10^{-5} and 1×10^{-4} Hartree for the reference and fragment energies at the MBE(1), MBE(2), and MBE(3) orders, respectively. The average $E_2(\text{noise})$ and $E_3(\text{noise})$ (denoted as $\langle E_2(\text{noise}) \rangle$ and $\langle E_3(\text{noise}) \rangle$),

respectively) and the corresponding standard deviations (denoted as σ_2 and σ_3 , respectively) with respect to different ϵ in each simulation are listed in Table IX. The results in Figure 9 and Table IX enable us to clearly draw three conclusions: (a), the energy deviations at the third order are significantly larger than those at the second order, attributed to the fact that the error accumulation increases significantly with the MBE order increases; (b), the energy deviations decreased with ϵ . However, the value of ϵ corresponds to $1/\sqrt{N_{\text{meas}}}$, where N_{meas} is the number of measurements, indicating that this is not an efficient way to control noise; (c), in the rightmost plot, the number of measurements corresponding to ϵ^* is actually less than that corresponding to $\epsilon = 2 \times 10^{-5}$ Hartree; however, its energy deviations are much smaller than those of $\epsilon = 5 \times 10^{-6}$ Hartree. This excellent performance demonstrates that the strategy of increasing the number of measurements at lower orders is effective. We strongly recommend the use of different numbers of measurements at different orders in all problem decomposition methods, including MBE.

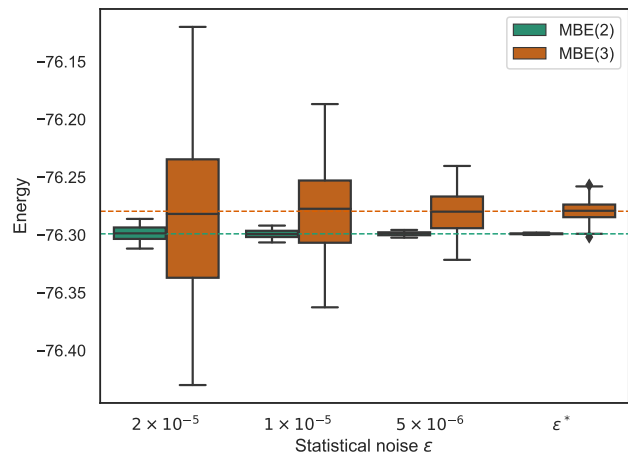


FIG. 9: Probability plot of the deviation of $E(\text{noise})$ from the exact energy with respect to different ϵ after 300 times simulations based on the MBE-FCI data of water with the aug-cc-pVDZ basis set.

V. CONCLUDING REMARKS

To deal with the constrained quantum resources in quantum computing, in this study, we combined VQE and VQD with the theoretical framework of MBE. To decompose the tested molecules into fragments by the expansion of secondary orbitals. Thereupon, we solved the ground state and excited states energies of each fragment by the VQE and VQD algorithms using the (same or different) UCC ansatz. The two approaches we adopted are denoted as MBE-UCCSD and MBE-UCCGSD/UCCpGSD, the latter of which uses the par-

TABLE IX: $\langle E_2(\text{noise}) \rangle$ and $\langle E_3(\text{noise}) \rangle$ and the corresponding σ_2 and σ_3 with respect to different ϵ after 300 times simulations based on the MBE-FCI data of water with the aug-cc-pVDZ basis set are listed. $\langle E_2(\text{noise}) \rangle$ and $\langle E_3(\text{noise}) \rangle$ are in a.u., σ_2 and σ_3 are in mH.

ϵ	$\langle E_2(\text{noise}) \rangle$	σ_2	$\langle E_3(\text{noise}) \rangle$	σ_3
2×10^{-5}	-76.29859	6.2	-76.28502	68.8
1×10^{-5}	-76.29917	3.3	-76.27816	36.6
5×10^{-6}	-76.29900	1.6	-76.27995	18.1
ϵ^*	-76.29902	0.4	-76.27938	7.8

tially generalized UCCGSD operator in the description of the fragment wavefunction and can be considered as an approximation to MBE-UCCGSD. The reference-unrelaxed approximation introduced in this work has demonstrated a significant reduction in the parameter-optimization burden during fragment computation. Furthermore, it was shown that the resulting error can be effectively suppressed by employing optimized orbitals. The ground state energies during the bond-breaking processes of two molecules (H_2O and N_2) and vertical excitation energies of three small molecules (LiH , CH^+ and H_2O) were investigated. MBE-UCCSD essentially aims for the UCCSD results with a large basis set and can provide satisfactory descriptions in single-reference systems; however, its performance has been shown to be inferior for multireference systems. In contrast, MBE-UCCGSD/UCCpGSD showed a stable and reliable ability to describe all tests, particularly for multireference systems. The results illustrate that the UCCGSD ansatz is necessary to describe the reference wavefunction which may include a strong static correlation, whereas the partially generalized UCCSD ansatz is sufficiently accurate to capture the dynamical correlation in the fragments. Considering the balance between the rapidly increasing computational cost as the MBE order increases and the accuracy of the results, we recommend using the reference-unrelaxed MBE(3)-UCCGSD/UCCpGSD with optimized orbitals for computing large systems in quantum computing.

We also designed a simulation to assess the effect of the inevitably present shot noise on the total energy. Our results showed that increasing the number of measurements at the lower orders is a highly efficient way to control the error introduced by shot noise, which can effectively suppress error accumulation without significantly increasing the cost. Finally, we anticipate that our framework could be effectively combined with preprocessing approaches, such as transcorrelated methods for quantum computing, which have been advancing rapidly, to achieve even greater accuracy.

ASSOCIATED CONTENT

Supporting information

The performance of the "reference-relaxed" MBE-UCC methods is shown in SI. The PESs for the bond dissociation processes of H_2O and N_2 described by MBE-UCCSD, MBE-UCCGSD/UCCpGSD and MRCI+Q are shown in Figures S1 and S2. Furthermore, the deviations of the second- and third-order MBE-UCC energies with respect to MRCI+Q are listed in Tables S1 and S2. Finally, the ground state energies and vertical excitation energies provided by MBE-UCCSD, MBE-UCCGSD/UCCpGSD and MBE-FCI for the three molecules (LiH , CH^+ and H_2O) are listed in Tables S3, S4 and S5, respectively.

ACKNOWLEDGMENTS

We wish to thank Siu Chung Tsang for continual computational support. This work was supported by JST, PRESTO (Grant Number JPMJPR2016), Japan. We gratefully acknowledge ECCSE, Kobe University and ACCMS, Kyoto University for their computational resources.

- ¹White, S. R. Density matrix formulation for quantum renormalization groups. *Phys. Rev. Lett.* **1992**, *69*, 2863–2866.
- ²Chan, G. K.-L.; Sharma, S. The Density Matrix Renormalization Group in Quantum Chemistry. *Annu. Rev. Phys. Chem.* **2011**, *62*, 465–481.
- ³Booth, G. H.; Thom, A. J. W.; Alavi, A. Fermion Monte Carlo without fixed nodes: A game of life, death, and annihilation in Slater determinant space. *J. Chem. Phys.* **2009**, *131*.
- ⁴Cleland, D.; Booth, G. H.; Alavi, A. Communications: Survival of the fittest: Accelerating convergence in full configuration-interaction quantum Monte Carlo. *J. Chem. Phys.* **2010**, *132*.
- ⁵Sugiyama, G.; Koonin, S. Auxiliary field Monte-Carlo for quantum many-body ground states. *Ann. Phys.* **1986**, *168*, 1–26.
- ⁶Xu, E.; Uejima, M.; Ten-no, S. L. Full Coupled-Cluster Reduction for Accurate Description of Strong Electron Correlation. *Phys. Rev. Lett.* **2018**, *121*, 113001.
- ⁷Xu, E.; Uejima, M.; Ten-no, S. L. Towards Near-Exact Solutions of Molecular Electronic Structure: Full Coupled-Cluster Reduction with a Second-Order Perturbative Correction. *J. Phys. Chem. Lett.* **2020**, *11*, 9775–9780.
- ⁸Holmes, A. A.; Changlani, H. J.; Umrigar, C. J. Efficient Heat-Bath Sampling in Fock Space. *J. Phys. Chem. Lett.* **2016**, *12*, 1561–1571.
- ⁹Liu, W.; Hoffmann, M. R. iCI: Iterative CI toward full CI. *J. Chem. Theory Comput.* **2016**, *12*, 1169–1178.
- ¹⁰Tubman, N. M.; Lee, J.; Takeshita, T. Y.; Head-Gordon, M.; Whaley, K. B. A deterministic alternative to the full configuration interaction quantum Monte Carlo method. *J. Chem. Phys.* **2016**, *145*.
- ¹¹Eriksen, J. J.; Lipparini, F.; Gauss, J. Virtual Orbital Many-Body Expansions: A Possible Route towards the Full Configuration Interaction Limit. *J. Phys. Chem. Lett.* **2017**, *8*, 4633.
- ¹²Eriksen, J. J.; Gauss, J. Generalized Many-Body Expanded Full Configuration Interaction Theory. *J. Phys. Chem. Lett.* **2019**, *10*, 7910.
- ¹³Manin, Y. *Computable and Noncomputable* (Sovetskoye Radio, Moscow, 1980), pp. 13–15 (in Russian).

- ¹⁴Feynman, R. P. Simulating physics with computers. *Int. J. Theor. Phys.* **1982**, *21*, 467.
- ¹⁵Lloyd, S. Universal Quantum Simulators. *Science* **1996**, *273*, 1073.
- ¹⁶Aspuru-Guzik, A.; Dutoi, A. D.; Love, P. J.; Head-Gordon, M. Simulated Quantum Computation of Molecular Energies. *Science* **2005**, *309*, 1704.
- ¹⁷Peruzzo, A.; McClean, J.; Shadbolt, P.; Yung, M.-H.; Zhou, X.-Q.; Love, P. J.; Aspuru-Guzik, A.; O'Brien, J. L. A variational eigenvalue solver on a photonic quantum processor. *Nat. Commun.* **2014**, *5*, 4213.
- ¹⁸O'Malley, P. J. J.; Babbush, R.; Kivlichan, I. D.; Romero, J.; McClean, J. R.; Barends, R.; Kelly, J.; Roushan, P.; Tranter, A.; Ding, N.; Campbell, B.; Chen, Y.; Chen, Z.; Chiaro, B.; Dunsworth, A.; Fowler, A. G.; Jeffrey, E.; Lucero, E.; Megrant, A.; Mutus, J. Y.; Neeley, M.; Neill, C.; Quintana, C.; Sank, D.; Vainsencher, A.; Wenner, J.; White, T. C.; Coveney, P. V.; Love, P. J.; Neven, H.; Aspuru-Guzik, A.; Martinis, J. M. Scalable Quantum Simulation of Molecular Energies. *Phys. Rev. X* **2016**, *6*, 031007.
- ¹⁹Kandala, A.; Mezzacapo, A.; Temme, K.; Takita, M.; Brink, M.; Chow, J. M.; Gambetta, J. M. Hardware-efficient variational quantum eigensolver for small molecules and quantum magnets. *Nature* **2017**, *549*, 242.
- ²⁰Hempel, C.; Maier, C.; Romero, J.; McClean, J.; Monz, T.; Shen, H.; Jurcevic, P.; Lanyon, B. P.; Love, P.; Babbush, R.; Aspuru-Guzik, A.; Blatt, R.; Roos, C. F. Quantum Chemistry Calculations on a Trapped-Ion Quantum Simulator. *Phys. Rev. X* **2018**, *8*, 031022.
- ²¹Fowler, A. G.; Mariantoni, M.; Martinis, J. M.; Cleland, A. N. Surface codes: Towards practical large-scale quantum computation. *Phys. Rev. A* **2012**, *86*, 032324.
- ²²Yoder, T. J.; Takagi, R.; Chuang, I. L. Universal Fault-Tolerant Gates on Concatenated Stabilizer Codes. *Phys. Rev. X* **2016**, *6*, 031039.
- ²³Fowler, A. G.; Gidney, C. Low overhead quantum computation using lattice surgery. **2019**, arXiv:1808.06709 [quant-ph], date of access: 2023/9/29.
- ²⁴Suzuki, Y.; Endo, S.; Fujii, K.; Tokunaga, Y. Quantum Error Mitigation as a Universal Error Reduction Technique: Applications from the NISQ to the Fault-Tolerant Quantum Computing Eras. *PRX Quantum* **2022**, *3*, 010345.
- ²⁵Ganzhorn, M.; Egger, D.; Barkoutsos, P.; Ollitrault, P.; Salis, G.; Moll, N.; Roth, M.; Fuhrer, A.; Mueller, P.; Werner, S.; Tavernelli, I.; Filipp, S. Gate-Efficient Simulation of Molecular Eigenstates on a Quantum Computer. *Phys. Rev. Appl.* **2019**, *11*, 044092.
- ²⁶Nakanishi, K. M.; Mitarai, K.; Fujii, K. Subspace-search variational quantum eigensolver for excited states. *Phys. Rev. Res.* **2019**, *1*, 033062.
- ²⁷Babbush, R.; Wiebe, N.; McClean, J.; McClain, J.; Neven, H.; Chan, G. K.-L. Low-Depth Quantum Simulation of Materials. *Phys. Rev. X* **2018**, *8*, 011044.
- ²⁸Kivlichan, I. D.; McClean, J.; Wiebe, N.; Gidney, C.; Aspuru-Guzik, A.; Chan, G. K.-L.; Babbush, R. Quantum Simulation of Electronic Structure with Linear Depth and Connectivity. *Phys. Rev. Lett.* **2018**, *120*, 110501.
- ²⁹Ryabinkin, I. G.; Yen, T.-C.; Genin, S. N.; Izmaylov, A. F. Qubit Coupled Cluster Method: A Systematic Approach to Quantum Chemistry on a Quantum Computer. *J. Chem. Theory Comput.* **2018**, *14*, 6317.
- ³⁰Grimsley, H. R.; Economou, S. E.; Barnes, E.; Mayhall, N. J. An adaptive variational algorithm for exact molecular simulations on a quantum computer. *Nat. Commun.* **2019**, *10*, 3007.
- ³¹Tsuchimochi, T.; Mori, Y.; Ten-no, S. L. Spin-projection for quantum computation: A low-depth approach to strong correlation. *Phys. Rev. Research* **2020**, *2*, 043142.
- ³²Tsuchimochi, T.; Taii, M.; Nishimaki, T.; Ten-no, S. L. Adaptive construction of shallower quantum circuits with quantum spin projection for fermionic systems. *Phys. Rev. Research* **2022**, *4*, 033100.
- ³³Bauman, N. P.; Bylaska, E. J.; Krishnamoorthy, S.; Low, G. H.; Wiebe, N.; Granade, C. E.; Roetteler, M.; Troyer, M.; Kowalski, K. Downfolding of many-body Hamiltonians using active-space models: Extension of the sub-system embedding sub-algebras approach to unitary coupled cluster formalisms. *J. Chem. Phys.* **2019**, *151*, 014107.
- ³⁴Bauman, N. P.; Low, G. H.; Kowalski, K. Quantum simulations of excited states with active-space downfolded Hamiltonians. *J. Chem. Phys.* **2019**, *151*, 234114.
- ³⁵McArdle, S.; Tew, D. P. Improving the accuracy of quantum computational chemistry using the transcorrelated method. **2020**, arXiv:2006.11181 [quant-ph], date of access: 2023/9/29.
- ³⁶Sokolov, I. O.; Dobrautz, W.; Luo, H.; Alavi, A.; Tavernelli, I. Orders of magnitude reduction in the computational overhead for quantum many-body problems on quantum computers via an exact transcorrelated method. **2023**, arXiv:2201.03049 [quant-ph], date of access: 2023/9/29.
- ³⁷Ten-no, S. L. Nonunitary projective transcorrelation theory inspired by the F12 ansatz. *J. Chem. Phys.* **2023**, in press.
- ³⁸Yanai, T.; Shiozaki, T. Canonical transcorrelated theory with projected Slater-type geminals. *The Journal of Chemical Physics* **2012**, *136*, 084107.
- ³⁹Kumar, A.; Asthana, A.; Masteran, C.; Valeev, E. F.; Zhang, Y.; Cincio, L.; Tretiak, S.; Dub, P. A. Quantum Simulation of Molecular Electronic States with a Transcorrelated Hamiltonian: Higher Accuracy with Fewer Qubits. *J. Chem. Theory Comput.* **2022**, *18*, 5312–5324.
- ⁴⁰Gordon, M. S.; Fedorov, D. G.; Pruitt, S. R.; Slipchenko, L. V. Fragmentation Methods: A Route to Accurate Calculations on Large Systems. *Chem. Rev.* **2012**, *112*, 632.
- ⁴¹Collins, M. A.; Bettens, R. P. A. Energy-Based Molecular Fragmentation Methods. *Chem. Rev.* **2015**, *115*, 5607.
- ⁴²Raghavachari, K.; Saha, A. Accurate Composite and Fragment-Based Quantum Chemical Models for Large Molecules. *Chem. Rev.* **2015**, *115*, 5643.
- ⁴³Sun, Q.; Chan, G. K.-L. Quantum Embedding Theories. *Acc. Chem. Res.* **2016**, *49*, 2705.
- ⁴⁴Verma, P.; Huntington, L.; Coons, M. P.; Kawashima, Y.; Yamazaki, T.; Zaribafiyani, A. Scaling up electronic structure calculations on quantum computers: The frozen natural orbital based method of increments. *J. Chem. Phys.* **2021**, *155*, 034110.
- ⁴⁵Fujii, K.; Mizuta, K.; Ueda, H.; Mitarai, K.; Mizukami, W.; Nakagawa, Y. O. Deep Variational Quantum Eigensolver: A Divide-And-Conquer Method for Solving a Larger Problem with Smaller Size Quantum Computers. *PRX Quantum* **2022**, *3*, 010346.
- ⁴⁶Yoshikawa, T.; Takanashi, T.; Nakai, H. Quantum Algorithm of the Divide-and-Conquer Unitary Coupled Cluster Method with a Variational Quantum Eigensolver. *Journal of Chemical Theory and Computation* **2022**, *18*, 5360–5373, PMID: 35926142.
- ⁴⁷Bethe, H. A.; Goldstone, J. Effect of a Repulsive Core in the Theory of Complex Nuclei. *Proc. R. Soc. A* **1957**, *238*, 551.
- ⁴⁸Nesbet, R. K. Atomic Bethe-Goldstone Equations. I. The Be Atom. *Phys. Rev.* **1967**, *155*, 51.
- ⁴⁹Nesbet, R. K. Atomic Bethe-Goldstone Equations. II. The Ne Atom. *Phys. Rev.* **1967**, *155*, 56.
- ⁵⁰Nesbet, R. K. Atomic Bethe-Goldstone Equations. III. Correlation Energies of Ground States of Be, B, C, N, O, F, and Ne. *Phys. Rev.* **1968**, *175*, 2.
- ⁵¹Zimmerman, P. M. Incremental full configuration interaction. *J. Chem. Phys.* **2017**, *146*, 104102.
- ⁵²Zimmerman, P. M. Singlet-Triplet Gaps through Incremental Full Configuration Interaction. *J. Phys. Chem. A* **2017**, *121*, 4712.
- ⁵³Zimmerman, P. M. Strong correlation in incremental full configuration interaction. *J. Chem. Phys.* **2017**, *146*, 224104.
- ⁵⁴Eriksen, J. J.; Gauss, J. Many-Body Expanded Full Configuration Interaction. I. Weakly Correlated Regime. *J. Chem. Theory Comput.* **2018**, *14*, 5180.

- ⁵⁵Eriksen, J. J.; Gauss, J. Many-Body Expanded Full Configuration Interaction. II. Strongly Correlated Regime. *J. Chem. Theory Comput.* **2019**, *15*, 4873.
- ⁵⁶Romero, J.; Babbush, R.; McClean, J. R.; Hempel, C.; Love, P. J.; Aspuru-Guzik, A. Strategies for quantum computing molecular energies using the unitary coupled cluster ansatz. *Quantum Sci. Technol.* **2018**, *4*, 014008.
- ⁵⁷Kühn, M.; Zanker, S.; Deglmann, P.; Marthaler, M.; Weiß, H. Accuracy and Resource Estimations for Quantum Chemistry on a Near-Term Quantum Computer. *J. Chem. Theory Comput.* **2019**, *15*, 4764.
- ⁵⁸Yoshikawa, T.; Takanashi, T.; Nakai, H. Quantum Algorithm of the Divide-and-Conquer Unitary Coupled Cluster Method with a Variational Quantum Eigensolver. *J. Chem. Theory Comput.* **2022**, *18*, 5360–5373.
- ⁵⁹Higgott, O.; Wang, D.; Brierley, S. Variational Quantum Computation of Excited States. *Quantum* **2019**, *3*, 156.
- ⁶⁰Eriksen, J. J.; Gauss, J. Ground and Excited State First-Order Properties in Many Body Expanded Full Configuration Interaction Theory. *J. Chem. Phys.* **2020**, *153*, 154107.
- ⁶¹Eriksen, J. J. The Shape of Full Configuration Interaction to Come. *J. Phys. Chem. Lett.* **2021**, *12*, 418.
- ⁶²Eriksen, J. J.; Gauss, J. Incremental treatments of the full configuration interaction problem. *WIREs Comput Mol Sci.* **2021**, *11*, e1525.
- ⁶³Nooijen, M. Can the Eigenstates of a Many-Body Hamiltonian Be Represented Exactly Using a General Two-Body Cluster Expansion? *Phys. Rev. Lett.* **2000**, *84*, 2108–2111.
- ⁶⁴Nakatsuji, H. Structure of the exact wave function. *J. Chem. Phys.* **2000**, *113*, 2949–2956.
- ⁶⁵Van Voorhis, T.; Head-Gordon, M. Two-body coupled cluster expansions. *J. Chem. Phys.* **2001**, *115*, 5033–5040.
- ⁶⁶Piecuch, P.; Kowalski, K.; Fan, P.-D.; Jedziniak, K. Exactness of Two-Body Cluster Expansions in Many-Body Quantum Theory. *Phys. Rev. Lett.* **2003**, *90*, 113001.
- ⁶⁷Davidson, E. R. Exactness of the General Two-Body Cluster Expansion in Many-Body Quantum Theory. *Phys. Rev. Lett.* **2003**, *91*, 123001.
- ⁶⁸Ronen, S. Can the Eigenstates of a Many-Body Hamiltonian Be Represented Exactly Using a General Two-Body Cluster Expansion? *Phys. Rev. Lett.* **2003**, *91*, 123002.
- ⁶⁹Mukherjee, D.; Kutzelnigg, W. Some comments on the coupled cluster with generalized singles and doubles (CCGSD) ansatz. *Chem. Phys. Lett.* **2004**, *397*, 174–179.
- ⁷⁰Lee, J.; Huggins, W. J.; Head-Gordon, M.; Whaley, K. B. Generalized Unitary Coupled Cluster Wave functions for Quantum Computation. *J. Chem. Theory Comput.* **2019**, *15*, 311–324.
- ⁷¹Hanauer, M.; Köhn, A. Pilot applications of internally contracted multireference coupled cluster theory, and how to choose the cluster operator properly. *J. Chem. Phys.* **2011**, *134*, 204111.
- ⁷²Debashish Mukherjee, R. K. M.; Mukhopadhyay, A. Applications of a non-perturbative many-body formalism to general open-shell atomic and molecular problems: calculation of the ground and the lowest $\pi - \pi^*$ singlet and triplet energies and the first ionization potential of trans-butadiene. *Mol. Phys.* **1977**, *33*, 955–969.
- ⁷³Yanai, T.; Chan, G. K. Canonical transformation theory for multireference problems. *J. Chem. Phys.* **2006**, *124*.
- ⁷⁴Evangelista, F. A.; Gauss, J. An orbital-invariant internally contracted multireference coupled cluster approach. *J. Chem. Phys.* **2011**, *134*.
- ⁷⁵Barkoutsos, P. K.; Gonthier, J. F.; Sokolov, I.; Moll, N.; Salis, G.; Fuhrer, A.; Ganzhorn, M.; Egger, D. J.; Troyer, M.; Mezzacapo, A.; Filipp, S.; Tavernelli, I. Quantum algorithms for electronic structure calculations: Particle-hole Hamiltonian and optimized wave-function expansions. *Phys. Rev. A* **2018**, *98*, 022322.
- ⁷⁶Moll, N.; Barkoutsos, P.; Bishop, L. S.; Chow, J. M.; Cross, A.; Egger, D. J.; Filipp, S.; Fuhrer, A.; Gambetta, J. M.; Ganzhorn, M.; Kandala, A.; Mezzacapo, A.; Müller, P.; Riess, W.; Salis, G.; Smolin, J.; Tavernelli, I.; Temme, K. Quantum optimization using variational algorithms on near-term quantum devices. *Quantum Sci. Technol.* **2018**, *3*, 030503.
- ⁷⁷Evangelista, F. A.; Chan, G. K.-L.; Scuseria, G. E. Exact parameterization of fermionic wave functions via unitary coupled cluster theory. *J. Chem. Phys.* **2019**, *151*, 244112.
- ⁷⁸Sokolov, I. O.; Barkoutsos, P. K.; Ollitrault, P. J.; Greenberg, D.; Rice, J.; Pistoia, M.; Tavernelli, I. Quantum orbital-optimized unitary coupled cluster methods in the strongly correlated regime: Can quantum algorithms outperform their classical equivalents? *J. Chem. Phys.* **2020**, *152*, 124107.
- ⁷⁹Sugisaki, K.; Kato, T.; Minato, Y.; Okuwaki, K.; Mochizuki, Y. Variational quantum eigensolver simulations with the multireference unitary coupled cluster ansatz: a case study of the C2v quasi-reaction pathway of beryllium insertion into a H2 molecule. *Phys. Chem. Chem. Phys.* **2022**, *24*, 8439–8452.
- ⁸⁰McClean, J. R.; Kimchi-Schwartz, M. E.; Carter, J.; de Jong, W. A. Hybrid quantum-classical hierarchy for mitigation of decoherence and determination of excited states. *Phys. Rev. A* **2017**, *95*, 042308.
- ⁸¹Colless, J. I.; Ramasesh, V. V.; Dahlen, D.; Blok, M. S.; Kimchi-Schwartz, M. E.; McClean, J. R.; Carter, J.; de Jong, W. A.; Siddiqi, I. Computation of Molecular Spectra on a Quantum Processor with an Error-Resilient Algorithm. *Phys. Rev. X* **2018**, *8*, 011021.
- ⁸²Higgott, O.; Wang, D.; Brierley, S. Variational Quantum Computation of Excited States. *Quantum* **2019**, *3*, 156.
- ⁸³Nakanishi, K. M.; Mitarai, K.; Fujii, K. Subspace-search variational quantum eigensolver for excited states. *Phys. Rev. Res.* **2019**, *1*, 033062.
- ⁸⁴Ollitrault, P. J.; Kandala, A.; Chen, C.-F.; Barkoutsos, P. K.; Mez zacapo, A.; Pistoia, M.; Sheldon, S.; Woerner, S.; Gambetta, J. M.; Tavernelli, I. v. Quantum equation of motion for computing molecular excitation energies on a noisy quantum processor. *Phys. Rev. Res.* **2020**, *2*, 043140.
- ⁸⁵Zhang, F.; Gomes, N.; Yao, Y.; Orth, P. P.; Iadecola, T. Adaptive variational quantum eigensolvers for highly excited states. *Phys. Rev. B* **2021**, *104*, 075159.
- ⁸⁶Tkachenko, N. V.; Zhang, Y.; Cincio, L.; Boldyrev, A. I.; Tretiak, S.; Dub, P. A. Quantum Davidson Algorithm for Excited States. **2022**, arXiv:2204.10741 [quant-ph], date of access: 2023/9/29.
- ⁸⁷Heya, K.; Nakanishi, K. M.; Mitarai, K.; Yan, Z.; Zuo, K.; Suzuki, Y.; Sugiyama, T.; Tamate, S.; Tabuchi, Y.; Fujii, K.; Nakamura, Y. Subspace variational quantum simulator. *Phys. Rev. Res.* **2023**, *5*, 023078.
- ⁸⁸Tsuchimochi, T.; Ryo, Y.; Ten-no, S. L.; Sasasako, K. Improved Algorithms of Quantum Imaginary Time Evolution for Ground and Excited States of Molecular Systems. *J. Chem. Theory Comput.* **2023**, *19*, 503–513.
- ⁸⁹Tsuchimochi, T.; Ryo, Y.; Ten-no, S. L. Multi-state quantum simulations via model-space quantum imaginary time evolution. **2022**, arXiv:2206.04494 [quant-ph], date of access: 2023/9/29.
- ⁹⁰Takahiro, Y.; Ten-no, S. L.; Tsuchimochi, T. Quantum Inverse Algorithm via Adaptive Variational Quantum Linear Solver: Applications to General Eigenstates. *J. Phys. Chem. A* **2023**, *127*, 6577–6592.
- ⁹¹Sokolov, I. O.; Barkoutsos, P. K.; Ollitrault, P. J.; Greenberg, D.; Rice, J.; Pistoia, M.; Tavernelli, I. Quantum orbital-optimized unitary coupled cluster methods in the strongly correlated regime: Can quantum algorithms outperform their classical equivalents? *J. Chem. Phys.* **2020**, *152*, 124107.
- ⁹²Mizukami, W.; Mitarai, K.; Nakagawa, Y. O.; Yamamoto, T.; Yan, T.; Ohnishi, Y.-y. Orbital optimized unitary coupled cluster theory for quantum computer. *Phys. Rev. Research* **2020**, *2*, 033421.
- ⁹³Tsuchimochi, T.; Mori, Y.; Shimomoto, Y.; Nishimaki, T.; Ryo, Y.; Taii, M.; Yoshikura, T.; Chung, T. S.; Sasasako, K.; Yoshimura, K. QuKET: the comprehensive quantum simulator for quantum chemistry. 2022; <https://github.com/quket/quket>,

- date of access: 2023/9/29.
- ⁹⁴ McClean, J. R.; Rubin, N. C.; Sung, K. J.; Kivlichan, I. D.; Bonet-Monroig, X.; Cao, Y.; Dai, C.; Fried, E. S.; Gidney, C.; Gimby, B.; Gokhale, P.; Häner, T.; Hardikar, T.; Havlíček, V.; Higgott, O.; Huang, C.; Izaac, J.; Jiang, Z.; Liu, X.; McArdle, S.; Neeley, M.; O’Brien, T.; O’Gorman, B.; Ozfidan, I.; Radin, M. D.; Romero, J.; Sawaya, N. P. D.; Senjean, B.; Setia, K.; Sim, S.; Steiger, D. S.; Steudtner, M.; Sun, Q.; Sun, W.; Wang, D.; Zhang, F.; Babbush, R. OpenFermion: the electronic structure package for quantum computers. *Quantum Sci. Technol.* **2020**, *5*, 034014.
- ⁹⁵ Sun, Q.; Berkelbach, T. C.; Blunt, N. S.; Booth, G. H.; Guo, S.; Li, Z.; Liu, J.; McClain, J. D.; Sayfutyarova, E. R.; Sharma, S.; Wouters, S.; Chan, G. K.-L. PySCF: the Python-based simulations of chemistry framework. *WIREs Comput Mol Sci.* **2018**, *8*, e1340.
- ⁹⁶ Suzuki, Y.; Kawase, Y.; Masumura, Y.; Hiraga, Y.; Nakadai, M.; Chen, J.; Nakanishi, K. M.; Mitarai, K.; Imai, R.; Tamiya, S.; Yamamoto, T.; Yan, T.; Kawakubo, T.; Nakagawa, Y. O.; Ibe, Y.; Zhang, Y.; Yamashita, H.; Yoshimura, H.; Hayashi, A.; Fujii, K. Qulacs: a fast and versatile quantum circuit simulator for research purpose. *Quantum* **2021**, *5*, 559.
- ⁹⁷ Jordan, P.; Wigner, E. *Z. Phys.* **1928**, *47*, 631.
- ⁹⁸ Bravyi, S.; Gambetta, J. M.; Mezzacapo, A.; Temme, K. Tapering off qubits to simulate fermionic Hamiltonians. **2017**, arXiv:1701.08213 [quant-ph], date of access: 2023/9/29.
- ⁹⁹ Setia, K.; Chen, R.; Rice, J. E.; Mezzacapo, A.; Pistoia, M.; Whitfield, J. D. Reducing Qubit Requirements for Quantum Simulations Using Molecular Point Group Symmetries. *J. Chem. Theory Comput.* **2020**, *16*, 6091–6097.
- ¹⁰⁰ Werner, H.; Knowles, P. J. An efficient internally contracted multiconfiguration–reference configuration interaction method. *J. Chem. Phys.* **1988**, *89*, 5803–5814.
- ¹⁰¹ An efficient method for the evaluation of coupling coefficients in configuration interaction calculations. *Chem. Phys. Lett.* **1988**, *145*, 514–522.
- ¹⁰² Pople, J. A.; Seeger, R.; Krishnan, R. Variational configuration interaction methods and comparison with perturbation theory. *Int. J. Quantum Chem.* **1977**, *12*, 149–163.
- ¹⁰³ Li, X.; Paldus, J. The general-model-space state-universal coupled-cluster method exemplified by the LiH molecule. *J. Chem. Phys.* **2003**, *119*, 5346–5357.
- ¹⁰⁴ Werner, H.-J.; Knowles, P. J.; Manby, F. R.; Black, J. A.; Doll, K.; Hefelmann, A.; Kats, D.; Köhn, A.; Korona, T.; Kreplin, D. A.; Ma, Q.; Miller, I.; Thomas F.; Mitrushchenkov, A.; Peterson, K. A.; Polyak, I.; Rauhut, G.; Sibaev, M. The Molpro quantum chemistry package. *J. Chem. Phys.* **2020**, *152*.
- ¹⁰⁵ Loos, P.-F.; Scemama, A.; Blondel, A.; Garniron, Y.; Cafarel, M.; Jacquemin, D. A Mountaineering Strategy to Excited States: Highly Accurate Reference Energies and Benchmarks. *J. Chem. Theory Comput.* **2018**, *14*, 4360–4379.